



Networked nanoconstrictions: An effective route to tuning the thermal transport properties of graphene



Bing-Yang Cao^{*}, Wen-Jun Yao, Zhen-Qiang Ye

Key Laboratory for Thermal Science and Power Engineering of Ministry of Education, Department of Engineering Mechanics, Tsinghua University, Beijing 100084, PR China

ARTICLE INFO

Article history:

Received 16 July 2015

Received in revised form

24 September 2015

Accepted 25 September 2015

Available online 30 September 2015

ABSTRACT

Tuning the thermal transport properties of graphene is under intense investigation to achieve novel material functionalities. Here we propose a strategy of networked nanoconstrictions to maintain the ultrahigh thermal conductivity like in design of graphene-based integrated circuits, or to reduce to the minimum for thermoelectrics of energy conversion. By using molecular dynamics simulations, we study the thermal transport behavior in the 18.2-nm-long graphene sheet and firstly report the characteristics of the thermal resistance arising from single-nanoconstriction, inversely proportional to the constriction width and independent of geometry shapes, which agrees well with the derived two-dimensional ballistic resistance model. After the nanoconstrictions are networked, the results elucidate a parallel relationship between ballistic resistances in parallel systems, and especially, a complicated superimposed effect of arrangement mode on ballistic resistances in series systems governed by the phonon localization and corresponding change of phonon transmission angle. Such anomalous phenomenon causes a decrease or further increase in the total ballistic resistance, e.g., tuning the thermal transport property of graphene as much as or more than 96% with specific nanoconstriction networks. We believe this feasible and versatile route will effectively expand potential applications of two-dimensional graphene and also pave the way for three-dimensional materials in the future.

© 2015 Elsevier Ltd. All rights reserved.

1. Introduction

Graphene, a two-dimensional material formed of the honeycomb lattice of sp^2 bonded carbon atoms, has been reported to show unique thermal properties, up to 5400 W/(m·K) demonstrated by Balandin et al. [1], since it first became experimentally accessible [1–8]. From a practical point of view, for designing ever-smaller integrated circuits and other graphene-based thermal components under complicated architectures, good thermal management and thermal signal processing, which means making full use of the ultrahigh thermal conductivity of graphene, can greatly improve their performance [3,8–10]. Meanwhile, there also have been attempts to decrease the thermal conductivity of graphene as much as possible and use it for thermoelectric energy conversion [5,11,12]. Considering all these potential applications, how to control the carrier transport or tune the thermal properties in a broader range becomes the key problem in the thermal research

community of graphene.

Researchers have increasingly focused on the available methods, including physical and chemical means [13–28]. And the most popular one to tune the thermal properties of graphene, or nearly any material, would be point defects engineering, such as vacancies or impurity doping. Increasing defect concentration could increase the strength of phonon scattering and lead to a large-scale reduction in thermal conductivity [13–15]. However, because its sensitivity to spatial distribution of defects, poor controllability is a problem and the thermal conductivity decreases slowly in the case of greater defect concentration [15]. What's more, the use of substitutional impurities would also degrade electron transport, thus it is unlikely to be a candidate for graphene-based thermoelectric application [13]. Chemical functionalization [16–20] is another popular method to suppress the thermal conductivity, it roughly includes covalent and non-covalent types, but may be countless if classified by modified atoms, atomic groups, or substrate. Graphene oxide is a low-cost and easy-to-get derivative during the mass production of graphene [18], hydrogenated graphene has also attracted considerable interest especially after the bandgap

^{*} Corresponding author.

E-mail address: caoby@tsinghua.edu.cn (B.-Y. Cao).

opening was experimentally observed by periodic modulations of the graphene and hydrogenated graphene lattice, called nanoroads [17,19]. But for other complex functional groups or physisorption, the challenges of reliable production with desired thermal conductivity and enough robustness corresponding to stable configuration are obstacles to overcome [16]. Isotope engineering directly affects the phonon mean free path (MFP) through phonon mass-difference scattering, but only a reduction in thermal conductivity by a factor of 2 is available [21,22]. Besides, researchers have also investigated the impacts from edge passivation [4,21], asymmetric geometry shape [23], strain [24] and grain-boundaries [25,26] on graphene. However, for applications where cheaper and more stable graphene sheet with tunable thermal properties in a broader range is needed, a simpler and more effective fabrication method is still highly desired.

Geometrical constriction at the nanoscale significantly affects the heat flow or carriers. Prasher et al. theoretically demonstrated that the thermal conductivity of a packed bed of crystalline spherical nanoparticles in a simple cubic arrangement can be smaller than the minimum thermal conductivity given by the Einstein limit [29] and later reported the related experimentally measured thermal conductivity of alumina nanoparticle packed beds which is only 35% higher than the thermal conductivity of air [30]. On these efforts, the significant reduction of the thermal conductivity and the high thermal resistance produced by the geometrical constriction between neighboring particles is pretty intriguing. Theoretically, for three-dimensional (3D) systems, if the characteristic size of the constriction (a) is much smaller than the phonon MFP in material (l), the diffusive thermal resistance of the constriction at the Maxwell's limit is given by the macroscopic constriction model $R_{d,3D} = 1/2ka$, where k is the thermal conductivity of material [31,32]. If in the other limit of $a \gg l$, phonon transport through the constriction will be ballistic and the ballistic resistance is calculated by integrating the ballistic phonon flux from different directions through the constriction [33],

$$R_{b,3D} = \frac{\Delta T}{J} = \left[\frac{A}{2} \int_0^\infty \int_0^{\pi/2} \frac{\partial \langle n \rangle}{\partial T} \hbar \omega D(\omega) v_g(\omega) \tau(\theta) \sin \theta d\theta d\omega \right]^{-1} = \frac{4}{A v_g c_v}, \quad (1)$$

where ΔT is the temperature difference, J is the heat flow, A is the area of the constriction, n is the occupation of phonons given by the Bose-Einstein distribution corresponding to the local temperature, \hbar is the reduced Planck constant, ω is the frequency of phonons, $D(\omega)$ is the phonon density of states, v_g is the phonon group velocity, $\tau(\theta)$ is the transmissivity of phonons, θ is the transmissivity angle and c_v is the specific heat per unit volume. For graphene, because of the long phonon MFP (0.5–1.0 μm [3,34,35]), the thermal transport across the geometrical constriction at the nanoscale will easily fall in the ballistic regime, and thus a ballistic resistance is introduced. The ballistic resistance of the single-constriction in graphene has been studied preliminarily, which is on the order of 10^7 – 10^9 K/W and suppresses the thermal conductivity dramatically [36,37]. But many problems still deserve to investigate, especially in operation of the practical engineering devices with not one but dense array of constrictions. Therefore, if we could know the performance of above ballistic constriction resistance much more clearly, the way of constructing the geometrical constriction maybe suggest a potential way to tune the thermal properties of graphene.

In this paper, we systematically investigate the influence of the thermal resistance at the nanoscale constriction on thermal transport in graphene using a non-equilibrium molecular dynamics

(NEMD) method, which agrees well with the analytical model for the ballistic resistance of single-constriction in two-dimensional nano-systems. More importantly, we further calculate the thermal transport properties of networked nanoconstrictions, and show that the staggered arrays enable a further reduction of thermal conductivity, which is from 0 to 100% in theory, and up to 96% among four typical systems with specific constriction network, because of the phonon localization. Thus, controlling the configuration of the embedded defects and constructing a nano-constriction network with reasonable arrangement suggest a feasible way to tune the thermal property of graphene for engineering applications.

2. Molecular dynamics simulations

2.1. Simulation details

We employed the NEMD method [38–41] and constructed a series of simulation systems, as illustrated in Fig. 1. Fig. 1a depicts the simplest system having one variable-width-constriction, constructed by introducing two linear vacancy defects in a pristine graphene sheet. The width of the geometrical constriction (w) varies from 0.65 nm to 8.42 nm, which is much smaller than the phonon MFP of graphene. Fig. 1b shows another single-constriction system with a changeable convex angle (φ), when φ is less than 180° , the graphene nanoribbons (GNRs) on either side of the constriction are trapezoidal, when φ is 180° , the system turns back into the rectangular one shown in Fig. 1a. Further, the simulation also performed on the systems with several sets of constrictions arranged in parallel, as shown in Fig. 1c, or in series, having different interval distance along the length direction (w_l) and different staggered distance along the width direction (w_w), as shown in Fig. 1d. All above simulation systems are originally 18.2-nm-long rectangular graphene sheets with zigzag long edges.

In the MD simulations, fixed boundary conditions are used at the outmost layers, i.e., the green atoms in Fig. 1, to prevent spurious rotation and translation of the system and free boundary conditions are used along the width direction. The heat current from the high-temperature slab (the red atoms) to the low-temperature slab (the blue atoms) is obtained by the velocity exchange method developed by Müller [42]. According to this method, the heat flow J is

$$J = \frac{\sum_{\text{transfers}} \frac{m}{2} (v_h^2 - v_c^2)}{t}, \quad (2)$$

in which m is the atomic mass of carbon, v_h is the velocity of the hottest atom in the low-temperature slab, v_c is the velocity of the coldest atom in the high-temperature slab, t is the statistical time. Specifically, by comparing the actual heat flow with the preset value, we can adjust the frequency of the velocity-exchange in real time and achieve that preset heat flow. Total energy and momentum of the system are conserved during the velocity-exchange, while the system temperature is kept at T_{ave} using the Nosé–Hoover thermostat method [43].

The C–C bonded interactions are modeled by the Brenner potential [44],

$$\phi = \sum_i \sum_{j(>i)} f(r_{ij}) [V_R(r_{ij}) - b_{ij} V_A(r_{ij})], \quad (3)$$

where ϕ is the total potential energy, V_R and V_A are the pair-additive repulsive and attractive potential terms, $f(r_{ij})$ is the truncation function that explicitly restricts the potential to nearest neighbors

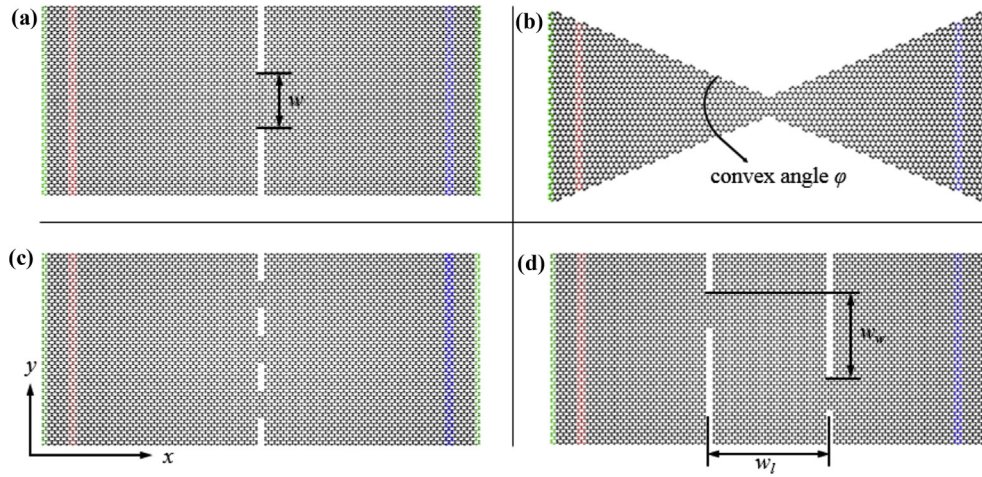


Fig. 1. Schematic of nanoconstriction structures in graphene by molecular dynamics simulation. (a) Rectangular, (b) trapezoidal, (c) parallel and (d) series simulation systems including high-temperature slabs (red) and low-temperature slabs (blue) with fixed boundaries (green), where system lengths are all 18.2 nm, widths of (a), (c) and (d) are 11.9 nm, w is the constriction width, φ is the convex angle, w_l is the interval distance and w_w is the staggered distance. (A colour version of this figure can be viewed online.)

and b_{ij} is the many-body interaction parameter. The atomic motion is integrated by the leap-frog scheme with a fixed time step of 0.5 fs. Each simulation case runs for 1 ns to reach a steady state, and then for 1.5 ns to average the temperature and heat flow over time. During the simulation, the system is equally divided into 50 slabs along the length direction, and the local instantaneous temperature for each slab, according to the energy equipartition theorem, is defined through the averaged kinetic energy as:

$$T_i = \frac{2}{3N_i k_B} \sum_{j=1}^{N_i} \frac{P_j^2}{2m}, \quad (4)$$

where N_i is the atom number of i -th slab, k_B is the Boltzmann constant and P_j is the momentum of the j -th atom.

2.2. Quantum correction

Since the Debye temperature of graphene is above 1000 K [45–48], when discussing the temperature properties of thermal resistance in low temperature region, it is necessary to add quantum correction to the kinetic energy computation of phonons. Specifically, making the total kinetic energy at local temperature T_{MD} equals to the half of the total phonon energy at quantum temperature T_q , according to gas kinetic theory and Debye model, we obtain the relationship between the corrected thermal resistance R_q and the simulated resistance R_{MD} , that is,

$$\frac{3}{2} N k_B T_{MD} = \frac{1}{2} \int_0^{k_B T_D / \hbar} \hbar \omega D(\omega) n(\omega, T_q) d\omega \quad (5)$$

$$\frac{R_q}{R_{MD}} = \frac{\partial T_q}{\partial T_{MD}}. \quad (6)$$

where $n(\omega, T_q) = 1/[\exp(\hbar\omega/k_B T_q) - 1]$ is the distribution function, $D(\omega) = 3\omega^2 V / (2\pi^2 v_g^3)$ is the phonon density of states, V is the volume, and $T_D = \hbar\omega_m / k_B$ is the Debye temperature, which is calculated from the Debye frequency $\omega_m = v_g (6\pi^2 N/V)^{1/3}$ and $1/v_g^3 = (1/v_l^3 + 1/v_t^3 + 1/v_z^3)/3$. Substituting the group velocity of three acoustic phonon branches $v_l = 21.04$ km/s, $v_t = 14.9$ km/s and $v_z = 2.5$ km/s [49] into above equations, we get the Debye temperature is 1035 K, close to the data in literature [45–48], and also

the relationship of correction factor $\partial T_q / \partial T_{MD}$ with the temperature in MD, shown in Fig. 2.

In Fig. 2, the correction factor decreases rapidly with the increasing temperature and finally converges to 1 in high temperature region. Thus, in this paper, it is necessary, especially in low temperature region, to correct the simulation results related to temperature by taking the quantum effects into account. Besides the temperature characteristics, effects of the heat flow, constriction width, convex angle and series or parallel arrangement on the constriction resistance are also investigated using the NEMD method. But in those cases, the system temperature T_{ave} is kept at 300 K, these concerns do not depend on the accurate value of temperature and we no longer do quantum correction to simulation results of these cases.

3. Results and discussions

The characteristics of the thermal resistance of the single-constriction in graphene are systematically studied using NEMD method and illustrated in Fig. 3. We first pay attention to the typical temperature profiles shown in Fig. 3a. As mentioned before, we produce an energy transfer from the high-temperature slab to the

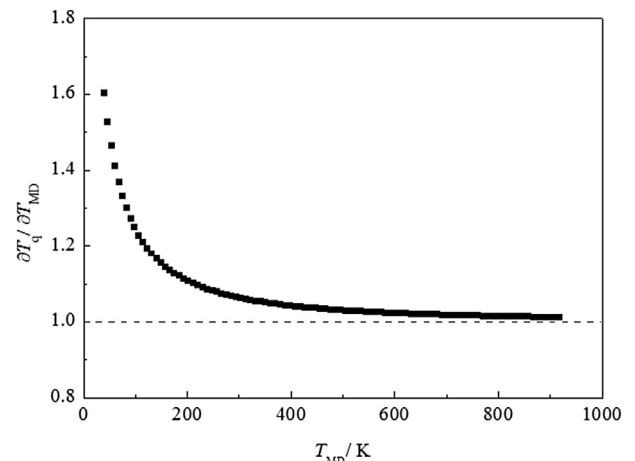


Fig. 2. Quantum correction factor for thermal resistance of graphene.

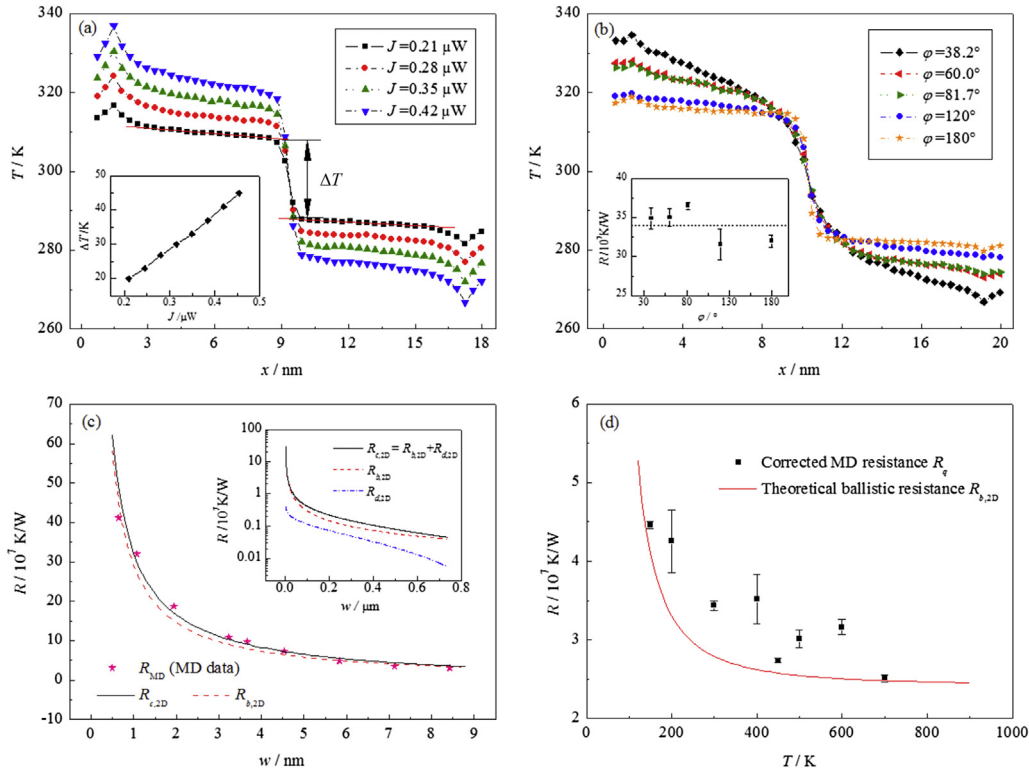


Fig. 3. Constriction thermal resistances of graphene single-constriction. (a) Temperature profiles of rectangular systems under different heat flows. The inset shows the temperature jump extracted from the temperature profiles versus the heat flow. (b) Temperature profiles of trapezoidal systems with different convex angle under a constant heat flow. The inset shows the constriction resistance versus the convex angle. (c) Constriction resistance as a function of constriction width. The inset shows the theoretical resistances of a 1- μm -wide graphene sheet. (d) Constriction resistance varying along with temperature. (A colour version of this figure can be viewed online.)

low-temperature slab by exchanging velocities. Thus, for each profile in Fig. 3a, there exists a linear temperature distribution between velocity-exchange slabs and the constriction, indicating a steady state of the simulation system, and a discontinuity at the constriction, indicating that energy is seriously blocked when passing through the constriction and an additional thermal resistance is introduced. In the following, we will mainly focus on this discontinuity, and similar to the interfacial thermal resistance, i.e., Kapitza resistance [50], the thermal resistance R at the constriction, which we called constriction resistance in this paper, is defined as

$$R = \frac{\Delta T}{J}, \quad (7)$$

where J and ΔT , respectively, correspond to the heat flow across the constriction and associated temperature jump at the constriction (as shown in Fig. 3a). The inset in Fig. 3a shows the dependence of the temperature jump ΔT extracted from temperature profiles on the heat flow. From four profiles of a single-constriction system under different heat flows and the inset in Fig. 3a, we can conclude that the trend of temperature profiles does not change as the heat flow increasing, while the temperature jump approximately increases linearly, which indicates that the constriction resistance is an intrinsic property of the system and it is independent of the heat flow. Thus in this paper, to reduce the error, the constriction resistance R is calculated by fitting the curve between temperature jump and the heat flow passing through the origin.

The geometrical constriction has been shown to introduce a constriction resistance in graphene. To further investigate the effect of the geometry shape in both sides of the constriction, we fix other parameters constant and only convex angle $\phi = 38.2^\circ, 60^\circ, 81.7^\circ,$

$120^\circ, 180^\circ$ are chosen (as shown in Fig. 1b), in order to reduce the effect of edge roughness. When the convex angle is 60° and 180° , the system contains two GNRs with edge chirality of armchair, and when convex angle is 120° , the edge chirality is zigzag. The calculated temperature profiles and corresponding constriction resistances of the variable-cross-section systems are shown in Fig. 3b. The line in the inset is the average of five values. We can see that the linear temperature distribution of the system with bigger convex angle is more gradual than that of smaller one, which is resulting from the decreased heat flux density with a wider width of each GNR slab under the same heat flow. But the thermal resistance is almost equal and varies only slightly as the convex angle changes, which indicates the constriction resistance is independent of the convex angle and insensitive to the detailed structure of constriction. This insensitivity is beneficial for popularization and utilization, and it is reasonable because the constriction resistance is a local value, which relates only to phonons passing through the constriction.

More interestingly, in Fig. 3c, with a fixed convex angle of 180° , the constriction resistance varies with the constriction width. This thermal transport behavior is distinctly different from that of the bulk material, which is independent of the size, and indicates the constriction resistance of graphene has obvious size effect. Specifically, with the constriction width increasing, which means the strength of the constriction weakening, the resistance decreases quickly from $4.12 \times 10^8 K/W$ to $3.00 \times 10^7 K/W$ and almost inversely proportional to the width of the constriction.

The analytical models of 3D constriction resistance have already been studied [31–33], but differently, constrictions constructed in graphene only on two dimensions (2D). Here, in analogy to the model of 3D ballistic resistance [33], we first model the 2D ballistic

resistance of the single-constriction by

$$R_{b,2D} = \frac{\Delta T}{J} = \left[\frac{2A}{\pi} \int_0^\infty \int_0^{\pi/2} \frac{\partial \langle n \rangle}{\partial T} \hbar \omega D(\omega) v_g(\omega) \tau(\theta) d\theta d\omega \right]^{-1} = \frac{\pi}{2W\delta v_g c_v}, \quad (8)$$

where $\delta = 0.335$ nm is the thickness of the graphene sheet [23,51]. In addition, Veziroglu et al. has deduced the 2D diffusive resistance [52], which is defined as

$$R_{d,2D} = \frac{2}{\pi k \delta} \ln \left[\left(\sin \frac{\pi W}{2l_y} \right)^{-1} \right] \quad (9)$$

where the thermal conductivity k of the pristine graphene sheet is calculated to be 128.40 W/(m·K), the width of the nanoribbon l_y is 11.9 nm, in this paper. Then, the total constriction resistance is $R_{c,2D} = R_{b,2D} + R_{d,2D}$, which has shown a good approximation with the rigorous solution of Boltzmann transport equation for electrons [53,54]. In the classical MD simulation without quantum corrections, the heat capacity per unit volume is $c_v = 3Nk_B/V$, in which N and V are the atom number and the volume of system, respectively. The effective phonon group velocity v_g is calculated according to section 2.2. With above parameters, the ballistic and total resistances are obtained and shown in Fig. 3c. Notably, they are nearly equal to each other and both agree well with the simulation results. Because the characteristic dimension of the constriction ranges from 0.65 nm to 8.42 nm, much smaller than the phonon MFP of graphene, the thermal transport across the constriction typically falls in a ballistic regime, and thus, the constriction resistance in this paper is mainly a ballistic resistance while the diffusive resistance is actually a small number can be ignored. Further, for other cases, the inset of Fig. 3c shows the theoretical resistance of a 1- μ m-wide graphene sheet with a bulk thermal conductivity of 3082 W/(m·K) [41], we can find that the ballistic resistance is always one or two orders of magnitude larger than the diffusive one. So, for a single-constriction with its constriction width much smaller than the MFP of graphene, it is feasible to ignore the diffusive resistance and predict the total constriction resistance with the model of the 2D ballistic resistance we proposed. And in the following, we will not distinguish the two concepts of constriction resistance and ballistic resistance. What's more, from Eq. (8), the theoretical ballistic resistance is independent of the heat-transfer condition and geometry shape of nanoribbon, while proportional to the reciprocal of the constriction width, which is consistent with the conclusion derived from MD results qualitatively.

Regard to the temperature characteristic of the ballistic resistance, the MD results in the cases with the constriction width of 7.13 nm are corrected according to section 2.2. As shown in Fig. 3d, the general trend is decreasing monotonically from 100 K to 900 K. Increasing temperature excites more phonons in high-frequency region and opens new transport channels across the constriction, and therefore lower thermal resistance. The curve in Fig. 3d is the analytical values of the 2D ballistic resistance model, and of them, the heat capacity at temperature T is calculated according to the Debye model

$$c_v(T) = \frac{1}{V} \int_0^\infty \hbar \omega D(\omega) \frac{\partial \langle n(\omega, T) \rangle}{\partial T} d\omega. \quad (10)$$

As shown, the curve agrees well with the simulation results. Above findings suggest that the 2D model is not only valid for the

performance about the geometry shape but also for describing the temperature characteristic of the single-constriction resistance in graphene.

Following above-mentioned basic features of the ballistic resistance in single-constriction graphene, we now focus on its superimposed effect of the networked constrictions that is more general in engineering applications. The systems depicted in Fig. 1c and d are two basic units of complicated network with abstraction and simplification. In Fig. 1c, several equal width constrictions and linear vacancy defects line up along the direction perpendicular to the heat flow, we call this system as a parallel system, and the relationship between the total ballistic resistance and the number of constrictions N is shown in Fig. 4. It is found that, the total ballistic resistance regardless of the width of each constriction is proportional to the inverse of the constriction number. Likewise, we also construct the parallel systems with different width constrictions and above conclusion is proven again. That is to say, it is a parallel relationship between these ballistic resistances in the parallel system, like electrical resistances in the parallel circuit, which agrees with the superposition principle of the diffusive constriction resistance or other thermal resistances in classical heat conduction. So, the total ballistic resistance in parallel systems is inversely proportional to the total constriction width, while independent of the constriction number or constriction distribution, and the 2D ballistic resistance model can be further improved into

$$R_{b,2D} = \frac{\pi}{2\delta v_g c_v \sum_{i=1}^N w_i}. \quad (11)$$

where w_i is the width of the i -th constriction.

Another basic unit of the constriction network, we call it series systems, is shown in Fig. 1d. As shown, several constrictions are arranged along the direction of the heat flow, with different interval distance along the length direction (w_l) and staggered distance along the width direction (w_w). In Fig. 5, R_{pro} is the previous ballistic resistance in the system where only one constriction exists, before being connected in series with another same-size constriction, and R_{ser} is the resistance of each constriction in the corresponding series system. It is generally known, in classical heat conduction, when thermal resistance are connected in series, they are linearly additive. But this common sense may fail when considering the ballistic resistance, as shown in Fig. 5. More specifically, we further classify series systems as in-line and staggered systems, according to whether the staggered distance w_w is zero or nonzero. For in-line

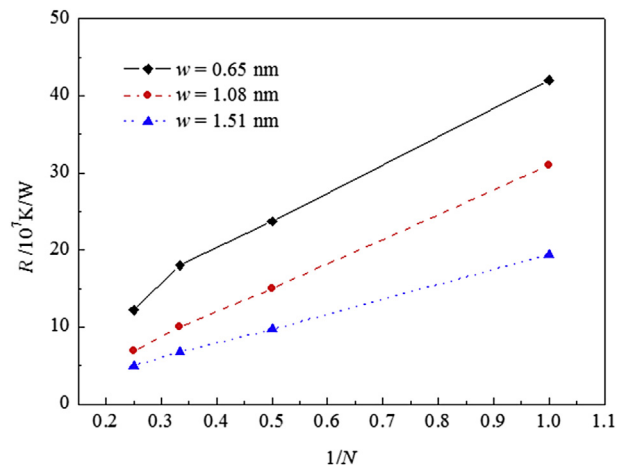


Fig. 4. Constriction thermal resistances of parallel systems as a function of constriction number. (A colour version of this figure can be viewed online.)

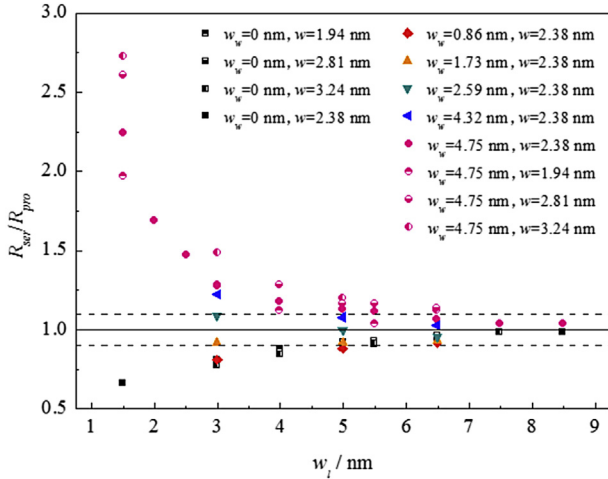


Fig. 5. Dimensionless constriction resistances of series systems as a function of interval distance. (A colour version of this figure can be viewed online.)

system, the staggered distance w_w is zero, from Fig. 5 we can see the dimensionless resistance R_{ser}/R_{pro} is related to the interval distance w_l and changes slightly with the constriction width. When the interval distance is less than 5 nm, the non-dimensional number is apparently lower than 1, indicating the interaction between constrictions significantly weakens the ballistic resistance in the in-line system. And as the interval distance increasing, the number is increased progressively to 1, indicating the interaction decreases gradually and disappears finally.

For staggered system, in addition to the interval distance, the staggered distance is another significant factor affecting the ballistic resistance. As shown in Fig. 5, when the staggered distance w_w is about less than 2 nm, the ballistic resistance is still reduced compared with the previous value and follows the same trend with the resistance in in-line system, which maybe resulted from the similar geometrical construction. But as the staggered distance increasing, the dimensionless number presents enlarging tendency and finally greater than 1. This anomalous phenomenon indicates that the interaction between constrictions could further restrict the energy transport when it passing through such constriction network. But as the staggered distance tends towards infinitude, or as interval distance increases, the dimensionless number is always coming progressively to 1, indicating the interaction decreases gradually and disappears finally. Besides, the dimensionless resistance also changes slightly with the constriction width. From above analyses, we have found that the total ballistic resistance in series systems is a combination of own factors and arrangement mode. And it diverges from the 2D ballistic resistance model to a certain extent. As the dotted lines in Fig. 5 shown, when the interval distance $w_l > 5$ nm, the deviation is less than 10% of the model, which is negligible in engineering application. But when $w_l < 5$ nm, the anomalous behavior of ballistic resistance is very noticeable.

The above anomalous interactions between ballistic resistances of networked nanoconstrictions could increase or further decrease the thermal transport properties of graphene, which motivates us to formally analyze the underlying microscopic mechanism. Here, we first compute the local heat flux of each atom in the series system, which defined as

$$q_i = V^{-1} \left[v_i E_i + \sum_{j \neq i} r_{ij} \left(-\frac{\partial \phi_j}{\partial r_i} \cdot v_i \right) \right]. \quad (12)$$

where q_i is the local heat flux of i -th atom, $E_i = m_i v_i \cdot v_i / 2 + \phi_i$ and $\phi_i = 1/2 \phi_{ij}$ are associated total energy and total potential energy, respectively. Then we calculate the distribution of the dimensionless number, i.e., q_i/q_{total} , in which q_{total} is the total heat flux. Similar analysis of cross-sectional heat flux distribution has been used to understand the edge effect on thermal transport in GNRs [55]. Fig. 6 illustrates the dimensionless local heat flux vector of the whole series system with verification that the total heat flow calculated from Eq. (12) is equal to the constant value imposed to the system according to Eq. (2). From the physical image of the heat conduction, it should be noted that the heat conduction not only affected by the constriction of geometry shape but also the arrangement mode, in agreement with previous simulation results.

In series systems, phonons propagating across or near constrictions are predominant heat carriers, while the lattice vibration of atoms far from constrictions cannot transport thermal energy as efficiently as the ones near constrictions, this phenomenon is called phonon localization [56,57]. First, for in-line systems, as shown in Fig. 6a and b, most phonons between two constrictions are localized, while effective phonons contributing to heat conduction travel across two constrictions directly with little or no scattering, which is known as the ballistic transport, and the angle of phonon transmission θ approaches zero. The phonon localization and the resulting ballistic transport between two constrictions cause a less suppression of heat conduction and a smaller resistance than that of the single-constriction. Second, for staggered systems, as shown in Fig. 6c and d, comparing with the in-line systems of same interval distance, the angle of phonon transmission θ is increased with the increasing channel length of the heat flow. And more importantly, the degree of phonon localization is reduced, while more phonons are involved, together with more phonon scattering, which means more suppression of heat conduction and a larger constriction resistance. Third, comparative analysis of several sets of in-line or staggered systems reveals that the smaller the interval distance is, the more phonons are localized, and interestingly, which means a smaller ballistic resistance for in-line system but a bigger ballistic resistance for staggered system.

The high ballistic resistances produced by the geometrical constriction are pretty intriguing. From the above analyses, the total constriction resistance of the systems containing single-constriction, constrictions connected in parallel or in series with the interval distance $w_l > 5$ nm, that we collectively call simple systems, could be calculated directly following the simple parallel or series relationship with enough accuracy, that is, for simple systems, the 2D ballistic resistance model is improved into

$$R_{b,2D} = \sum_{j=1}^M \frac{\pi}{2\delta v_g c_v \sum_{i=1}^{N_j} w_i}. \quad (13)$$

here, N and M are numbers of the constrictions connected in parallel and in series, respectively. From the above model we can see, the constriction width w , constriction numbers N and M combine to determine the total ballistic resistance introduced in simple systems. But for different 2D materials, the thermal properties of themselves could also be considered. Further, the effective thermal conductivity of the simple system could be calculated directly according to the 2D model,

$$\sigma = \left[\frac{1}{k} + \frac{l_y \delta}{l_x} R_{b,2D} \right]^{-1} = \left[\frac{1}{k} + \frac{l_y \delta}{l_x} \sum_{j=1}^M \frac{\pi}{2\delta v_g c_v \sum_{i=1}^{N_j} w_i} \right]^{-1}. \quad (14)$$

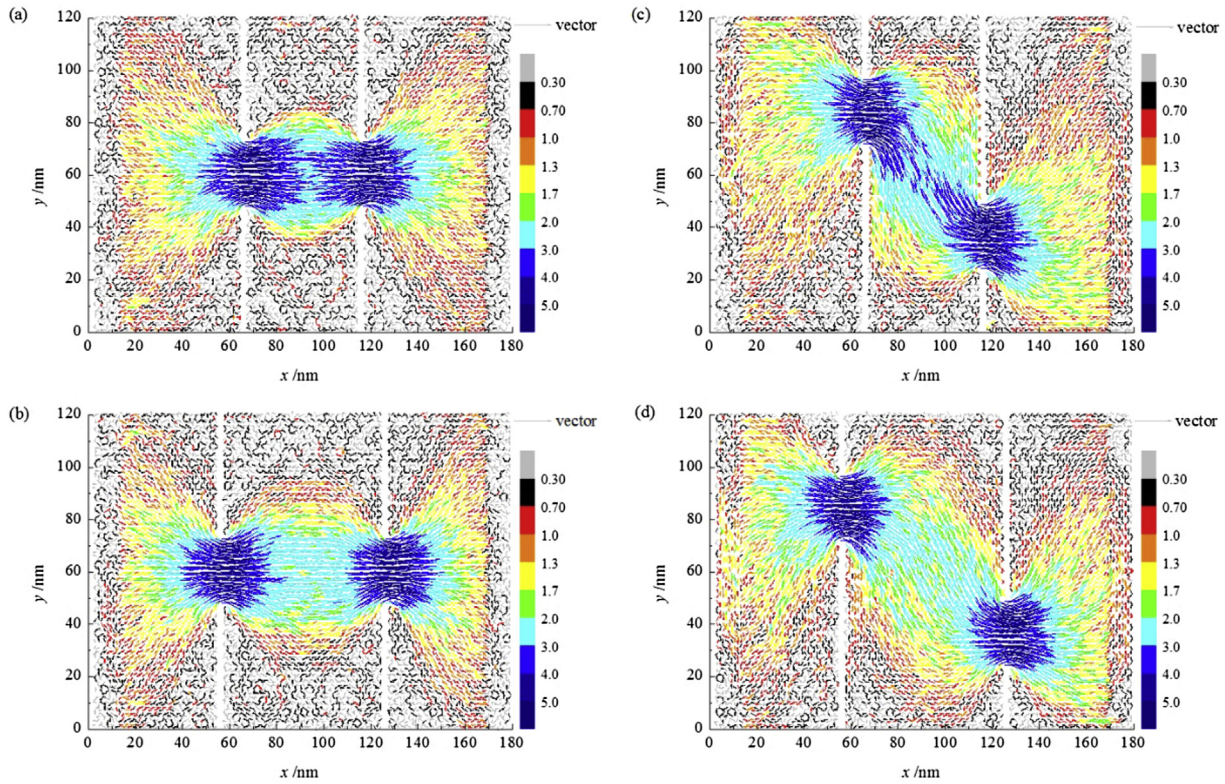


Fig. 6. Local heat flux profile of the in-line system with interval distance of (a) 4.99 nm and (b) 6.98 nm, and the staggered system with interval distance of (c) 4.99 nm and (d) 6.98 nm. (A colour version of this figure can be viewed online.)

here l_x is the system length, l_y is the system width, $k = 128.40 \text{ W}/(\text{m}\cdot\text{K})$ is the thermal conductivity of the pristine GNR in this paper, which is 18.2 nm long and 11.9 nm wide. According to Eqs. (13) and (14), the effect of the constriction number in parallel N and the constriction width w could be regarded as a whole. Thus, without loss of generality, assuming N_j equals 1 and each constriction connected in series is of equal size w , the theoretical thermal conductivity of the simple system with M constrictions is shown in Fig. 7. As shown, the most dominant factor is the constriction width which could reduce the thermal conductivity infinitely as the constriction width tends to zero in theory, but the minimum value

is limited by the system robustness corresponding to a stable configuration. What's more, with fixed constriction width, every increase of a constriction will reduce the thermal conductivity of simple system by about half. But similarly, the system length determines the maximum number of series constrictions, hence, the minimum value of the thermal conductivity. In addition, the points in Fig. 7 are prediction values of complex systems, which contain series constrictions with the interval distance $w_l < 5 \text{ nm}$, and the $R_{b,2D}$ in Eq. (14) is replaced by the MD results in Fig. 5. As shown in Fig. 7, the thermal conductivity of complex systems, ranged from 0.78 $\text{W}/(\text{m}\cdot\text{K})$ to 1.04 $\text{W}/(\text{m}\cdot\text{K})$, is even lower than that of the simple systems with other parameters unchanged, which demonstrates how the phonon localization further suppresses the heat conduction and reduces the thermal conductivity by orders of magnitude.

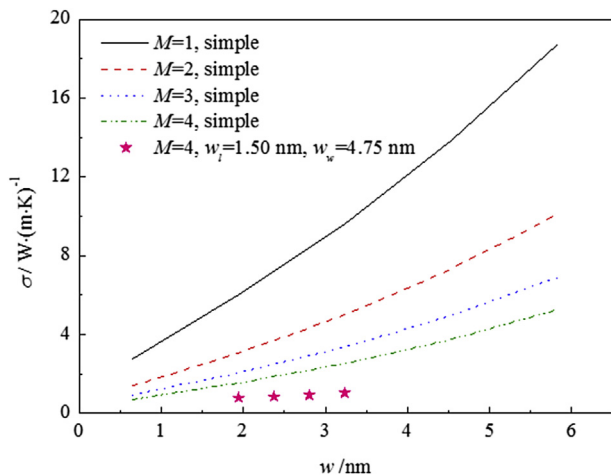



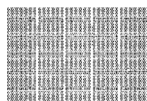


Fig. 7. Effective thermal conductivity of 18.2-nm-long and 11.9-nm-wide nano-constriction network. (A colour version of this figure can be viewed online.)

Likewise, the MD results σ_{MD} and theoretically predictive thermal conductivities $\sigma_{prediction}$ calculated from Eq. (14) of four typical cases with same system size are shown in Table 1, where the reduction ratio is defined as $1 - \sigma_{MD}/k$. As shown, the MD thermal conductivities of the former three simple systems are 13.46 $\text{W}/(\text{m}\cdot\text{K})$ –33.55 $\text{W}/(\text{m}\cdot\text{K})$, which are reduced by about 70%–90%, in accordance with the prediction, while the thermal conductivity of the fourth complex system is 4.53 $\text{W}/(\text{m}\cdot\text{K})$, which is reduced by as much as 96% because of the specific arrangement. This thermal conductivity is lower than the minimum value of the reduced graphene oxide films and compatible with that of the graphene oxide films measured by Renteria et al. [28], and about three order of magnitude lower than the bulk graphene [1,41]. Thus, the combined effect of the above three factors, i.e., the constriction width, constriction number and arrangement mode, provides a tunable thermal conductivity over a wide range, also endless possibilities of graphene for engineering applications. For instance, if as

Table 1
Effective thermal conductivity of four typical constriction networks.

	Case1	Case2	Case3	Case4
Network schematic				
σ_{MD} (W/(m·K))	33.55	13.99	13.46	4.53
Reduction ratio	74%	89%	90%	96%
$\sigma_{prediction}$ (W/(m·K))	35.07	14.29	14.29	6.42
MD-prediction deviation	4%	2%	6%	29%

thermoelectric materials, researchers have demonstrated that defects can modify the local electronic band structure near Dirac points and endow graphene with a semiconductor behavior [58–61], and some graphene nanostructures [62–64] can degrade the thermal conductance but preserve the excellent electronic conduction, which may benefit the thermoelectric properties of graphene. Chang et al. [62] demonstrated that drilling nanopores in graphene interior does not affect edge charge currents while drastically reducing the phonon heat current. The combination of these two effects can yield highly efficient thermoelectric devices with maximum figure of merit $ZT = 5$. Bai et al. [63] has fabricated another new graphene nanostructure called graphene nanomesh, which is similar to the constriction network in shape, and demonstrated that the on-state electrical conductivity of the nanomesh of 7-nm or 10-nm neck width (the smallest dimension between two neighboring nanoholes) is comparable to that of the similar width GNRs [65]. Therefore, if connecting the nanoconstrictions in staggered and keeping the smallest constriction width unchanged, it is possible to decrease the thermal properties but preserve the electrical conductivity of graphene, and maybe suggest a higher thermoelectric figure of merit, which needs to be confirmed in the future. In a word, tuning the thermal transport properties via networked nanoconstrictions is a feasible and versatile method, and it broadens the range of the thermal conductivity of graphene, or nearly any material, and realizes the accurate control according to the constriction resistance model, which will expand potential applications of 2D graphene and also pave the way for 3D materials in the future.

4. Conclusion

In this paper, we comprehensively investigate the influence of the thermal resistance at the nanoscale constriction on thermal transport in 18.2-nm-long graphene using the NEMD method. For the single-nanoconstriction, it is found that the ballistic resistance is inversely proportional to the constriction width ranged from 0.65 nm to 8.42 nm, and decreases with the increasing temperature, while independent of the heat-transfer condition and detailed shape of the constriction. Further, when constrictions are networked, the interaction between constrictions will have a complicated effect on the ballistic resistance. In the parallel systems, the results show a parallel relationship between ballistic resistances, that is, the total resistance is inversely proportional to the total constriction width, while independent of the distribution. But for the series systems, another basic unit of constriction network, the total ballistic resistance is a combination of own factors and arrangement mode, and it diverges from the 2D ballistic resistance model to some extent. When the interval distance is smaller than 5 nm, the interaction between constrictions significantly weakens the ballistic resistance in in-line system and strengthens the resistance in staggered system with a larger staggered distance. But whether the staggered distance be large or small, as the interval

distance increasing, the resistance is always coming progressively to the previous value, indicating the interaction decreases gradually and disappears finally. By calculating the local heat flux vector, such anomalous phenomenon is mainly attributed to the phonon localization and corresponding changes of phonon transmission angle. Thus, making reasonable use of the constriction network is a potential and effective way to tune the thermal property of graphene, even 3D materials, over a wide range.

Acknowledgment

This work was supported by the National Natural Science Foundation of China (Grant Nos. 51322603, 51136001, 51356001), Science Fund for Creative Research Groups (No. 51321002), the Program for New Century Excellent Talents in University, Tsinghua University Initiative Scientific Research Program, and the Tsinghua National Laboratory for Information Science and Technology of China.

References

- [1] A.A. Balandin, S. Ghosh, W. Bao, I. Calizo, D. Teweldebrhan, F. Miao, et al., Superior thermal conductivity of single-layer graphene, *Nano Lett.* 8 (3) (2008) 902–907.
- [2] K.S. Novoselov, A.K. Geim, S.V. Morozov, D. Jiang, Y. Zhang, S.V. Dubonos, et al., Electric field effect in atomically thin carbon films, *Science* 306 (5696) (2004) 666–669.
- [3] S. Ghosh, I. Calizo, D. Teweldebrhan, E.P. Pokatilov, D.L. Nika, A.A. Balandin, et al., Extremely high thermal conductivity of graphene: prospects for thermal management applications in nanoelectronic circuits, *Appl. Phys. Lett.* 92 (15) (2008) 151911-1–151911-3.
- [4] D.L. Nika, E.P. Pokatilov, A.S. Askerov, A.A. Balandin, Phonon thermal conduction in graphene: role of umklapp and edge roughness scattering, *Phys. Rev. B* 79 (15) (2009) 155413–155421–12.
- [5] J.H. Seol, I. Jo, A.L. Moore, L. Lindsay, Z.H. Aitken, M.T. Pettes, et al., Two-dimensional phonon transport in supported graphene, *Science* 328 (5975) (2010) 213–216.
- [6] A.A. Balandin, Thermal properties of graphene and nanostructured carbon materials, *Nat. Mater.* 10 (8) (2011) 569–581.
- [7] D.L. Nika, A.A. Balandin, Two-dimensional phonon transport in graphene, *J. Phys. Condens. Matter* 24 (23) (2012) 233203–233211–18.
- [8] Z. Yan, D.L. Nika, A.A. Balandin, Thermal properties of graphene and few-layer graphene: applications in electronics, *IET Circ. Device Syst.* 9 (1) (2015) 4–12.
- [9] A.K. Geim, P. Kim, Carbon wonderland, *Sci. Am.* 298 (4) (2008) 90–97.
- [10] C. Soldano, A. Mahmood, E. Dujardin, Production, properties and potential of graphene, *Carbon* 48 (8) (2010) 2127–2150.
- [11] D. Dragoman, M. Dragoman, Giant thermoelectric effect in graphene, *Appl. Phys. Lett.* 91 (20) (2007) 203116–203121–3.
- [12] Y.M. Zuev, W. Chang, P. Kim, Thermoelectric and magnetothermoelectric transport measurements of graphene, *Phys. Rev. Lett.* 102 (9) (2009) 096807–096811–4.
- [13] J. Haskins, A. Kınacı, C. Sevik, H. Sevinçli, G. Cuniberti, T. Çağın, Control of thermal and electronic transport in defect-engineered graphene nanoribbons, *ACS Nano* 5 (5) (2011) 3779–3787.
- [14] J.W. Jiang, B.S. Wang, J.S. Wang, First principle study of the thermal conduction in graphene nanoribbon with vacancy and substitutional silicon defects, *Appl. Phys. Lett.* 98 (11) (2011) 113114–113121–3.
- [15] T.Y. Ng, J.J. Yeo, Z.S. Liu, A molecular dynamics study of the thermal conductivity of graphene nanoribbons containing dispersed Stone–Thrower–Wales defects, *Carbon* 50 (13) (2012) 4887–4893.
- [16] D.W. Boukhvalov, M.I. Katsnelson, Chemical functionalization of graphene,

- J. Phys. Condens Matter 21 (34) (2009) 344205–344211–12.
- [17] A.K. Singh, B.I. Yakobson, Electronics and magnetism of patterned graphene nanoroads, *Nano Lett.* 9 (4) (2009) 1540–1543.
- [18] B.Y. Zhu, S. Murali, W. Cai, X. Li, J.W. Suk, J.R. Potts, et al., Graphene and graphene oxide: synthesis, properties, and applications, *Adv. Mater.* 22 (35) (2010) 3906–3924.
- [19] S.K. Chien, Y.T. Yang, C.K. Chen, Influence of hydrogen functionalization on thermal conductivity of graphene: nonequilibrium molecular dynamics simulations, *Appl. Phys. Lett.* 98 (3) (2011) 033107–033111–3.
- [20] V. Georgakilas, M. Otyepka, A.B. Bourlinos, V. Chandra, N. Kim, K.C. Kemp, et al., Functionalization of graphene: covalent and non-covalent approaches, derivatives and applications, *Chem. Rev.* 112 (10) (2012) 6156–6214.
- [21] J. Hu, S. Schiffl, A. Vallabhaneni, X. Ruan, Y.P. Chen, Tuning the thermal conductivity of graphene nanoribbons by edge passivation and isotope engineering: a molecular dynamics study, *Appl. Phys. Lett.* 97 (13) (2010) 133107–133111–3.
- [22] S. Chen, Q. Wu, C. Mishra, J. Kang, H. Zhang, K. Cho, et al., Thermal conductivity of isotopically modified graphene, *Nat. Mater.* 11 (3) (2012) 203–207.
- [23] J. Hu, X. Ruan, Y.P. Chen, Thermal conductivity and thermal rectification in graphene nanoribbons: a molecular dynamics study, *Nano Lett.* 9 (7) (2009) 2730–2735.
- [24] N. Wei, L. Xu, H.Q. Wang, J.C. Zheng, Strain engineering of thermal conductivity in graphene sheets and nanoribbons: a demonstration of magic flexibility, *Nanotechnology* 22 (10) (2011) 105705–105711–11.
- [25] P.Y. Huang, C.S. Ruiz-Vargas, A.M. van der Zande, W.S. Whitney, M.P. Levendorf, J.W. Kevek, et al., Grains and grain boundaries in single-layer graphene atomic patchwork quilts, *Nature* 469 (7330) (2011) 389–393.
- [26] A.Y. Serov, Z.Y. Ong, E. Pop, Effect of grain boundaries on thermal transport in graphene, *Appl. Phys. Lett.* 102 (3) (2013) 033104–033111–5.
- [27] H. Malekpour, K.H. Chang, J.C. Chen, C.Y. Lu, D.L. Nika, K.S. Novoselov, et al., Thermal conductivity of graphene laminate, *Nano Lett.* 14 (9) (2014) 5155–5161.
- [28] J.D. Renteria, S. Ramirez, H. Malekpour, B. Alonso, A. Centeno, A. Zurutuza, et al., Strongly anisotropic thermal conductivity of free-standing reduced graphene oxide films annealed at high temperature, *Adv. Funct. Mater.* 25 (29) (2015) 4664–4672.
- [29] R. Prasher, Ultralow thermal conductivity of a packed bed of crystalline nanoparticles: a theoretical study, *Phys. Rev. B* 74 (16) (2006) 165413–165421–5.
- [30] X.J. Hu, R. Prasher, K. Lofgreen, Ultralow thermal conductivity of nanoparticle packed bed, *Appl. Phys. Lett.* 91 (20) (2007) 203113–203121–3.
- [31] M.G. Cooper, B.B. Mikic, M.M. Yovanovich, Thermal contact conductance, *Int. J. Heat. Mass Transf.* 12 (1969) 279–300.
- [32] C.V. Madhusudana, *Thermal Contact Conductance*, Springer, New York, 1996, pp. 1–43.
- [33] R. Prasher, Predicting the thermal resistance of nanosized constrictions, *Nano Lett.* 5 (11) (2005) 2155–2159.
- [34] B. Qiu, X. Ruan, Molecular dynamics simulations of thermal conductivity and spectral phonon relaxation time in suspended and supported graphene, *Appl. Phys. Lett.* 100 (19) (2012) 193101–1–193101–10.
- [35] S.J. Mahdizadeh, E.K. Goharshadi, Thermal conductivity and heat transport properties of graphene nanoribbons, *J. Nanopart. Res.* 16 (8) (2014) 2553–2561–12.
- [36] W.J. Yao, B.Y. Cao, H.M. Yun, B.M. Chen, Effects of nanosized constriction on thermal transport properties of graphene, *Nanoscale Res. Lett.* 9 (33) (2014) 408–411–7.
- [37] W.J. Yao, B.Y. Cao, Molecular dynamics studies on ballistic thermal resistance of graphene nano-junctions, *Commun. Theor. Phys.* 63 (5) (2015) 619–624.
- [38] B.Y. Cao, Y.W. Li, A uniform source-and-sink scheme for calculating thermal conductivity by nonequilibrium molecular dynamics, *J. Chem. Phys.* 133 (2) (2010) 024106–024111–5.
- [39] G.J. Hu, B.Y. Cao, Thermal resistance between crossed carbon nanotubes: molecular dynamics simulations and analytical modeling, *J. Appl. Phys.* 114 (22) (2013) 224308–224311–8.
- [40] Z. Ye, B. Cao, Z. Guo, High and anisotropic thermal conductivity of body-centered tetragonal C₄ calculated using molecular dynamics, *Carbon* 66 (2) (2014) 567–575.
- [41] W.J. Yao, B.Y. Cao, Thermal wave propagation in graphene studied by molecular dynamics simulations, *Chin. Sci. Bull.* 59 (27) (2014) 3495–3503.
- [42] F. Müller-Plathe, A simple nonequilibrium molecular dynamics method for calculating the thermal conductivity, *J. Chem. Phys.* 106 (14) (1997) 6082–6085.
- [43] W.G. Hoover, Canonical dynamics: equilibrium phase-space distributions, *Phys. Rev. A* 31 (3) (1985) 1695–1697.
- [44] D.W. Brenner, Empirical potential for hydrocarbons for use in simulating the chemical vapor deposition of diamond films, *Phys. Rev. B* 42 (15) (1990) 9458–9471.
- [45] T. Tohei, A. Kuwabara, F. Oba, I. Tanaka, Debye temperature and stiffness of carbon and boron nitride polymorphs from first principles calculations, *Phys. Rev. B* 73 (6) (2006) 064304–064311–6.
- [46] L.A. Falkovsky, Unusual field and temperature dependence of the Hall effect in graphene, *Phys. Rev. B* 75 (3) (2007) 033409–033411–4.
- [47] N. Yang, G. Zhang, B. Li, Thermal rectification in asymmetric graphene ribbons, *Appl. Phys. Lett.* 95 (3) (2009) 033107–033111–3.
- [48] A.I. Cocemasov, D.L. Nika, A.A. Balandin, Engineering of the thermodynamic properties of bilayer graphene by atomic plane rotations: the role of the out-of-plane phonons, *Nanoscale* 7 (30) (2015) 12851–12859.
- [49] Z.Q. Ye, B.Y. Cao, Z.Y. Guo, Study on thermal characteristics of phonons in graphene, *Acta Phys. Sin.* 63 (15) (2014) 54704–54711–7 (in Chinese).
- [50] E.T. Swartz, R.O. Pohl, Thermal boundary resistance, *Rev. Mod. Phys.* 61 (1989) 605–668.
- [51] E. Pop, V. Varshney, A.K. Roy, Thermal properties of graphene: fundamentals and applications, *MRS Bull.* 37 (12) (2012) 1273–1281.
- [52] T.N. Veziroglu, S. Chandra, Thermal conductance of two-dimensional constrictions, *Therm. Des. Princ. Spacecr. Entry Bodies* (1969) 591–615.
- [53] B. Nikolic, P.B. Allen, Electron transport through a circular constriction, *Phys. Rev. B* 60 (6) (1999) 3963–3969.
- [54] M.J.M. de Jong, Transition from Sharvin to Drude resistance in high-mobility wires, *Phys. Rev. B* 49 (11) (1994) 7778–7781.
- [55] Y. Wang, B. Qiu, X. Ruan, Edge effect on thermal transport in graphene nanoribbons: a phonon localization mechanism beyond edge roughness scattering, *Appl. Phys. Lett.* 101 (1) (2012) 013101–1–013101–4.
- [56] Y. Wang, A. Vallabhaneni, J. Hu, B. Qiu, Y.P. Chen, X. Ruan, Phonon lateral confinement enables thermal rectification in asymmetric single-material nanostructures, *Nano Lett.* 14 (2) (2014) 592–596.
- [57] J.W. Jiang, J. Lan, J.S. Wang, B. Li, Isotopic effects on the thermal conductivity of graphene nanoribbons: localization mechanism, *J. Appl. Phys.* 107 (5) (2010) 054314–054321–5.
- [58] J.M. Carlsson, M. Scheffler, Structural, electronic, and chemical properties of nanoporous carbon, *Phys. Rev. Lett.* 96 (4) (2006) 046806–046811–4.
- [59] J. Kang, J. Bang, B. Ryu, K.J. Chang, Effect of atomic-scale defects on the low-energy electronic structure of graphene: perturbation theory and local-density-functional calculations, *Phys. Rev. B* 77 (11) (2008) 115453–115461–9.
- [60] D.J. Appelhans, L.D. Carr, M.T. Lusk, Embedded ribbons of graphene allotropes: an extended defect perspective, *New J. Phys.* 12 (12) (2010) 125006.
- [61] T. Feng, X. Ruan, Z. Ye, B. Cao, Spectral phonon mean free path and thermal conductivity accumulation in defected graphene: the effects of defect type and concentration, *Phys. Rev. B* 91 (22) (2015) 224301–1–224301–12.
- [62] P.H. Chang, B.K. Nikolić, Edge currents and nanopore arrays in zigzag and chiral graphene nanoribbons as a route toward high-Z T thermoelectrics, *Phys. Rev. B* 86 (4) (2012) 041406–041411–5.
- [63] J. Bai, X. Zhong, S. Jiang, Y. Huang, X. Duan, Graphene nanomesh, *Nat. Nanotechnol.* 5 (3) (2010) 190–194.
- [64] L. Liang, E. Cruz-Silva, E.C. Girão, V. Meunier, Enhanced thermoelectric figure of merit in assembled graphene nanoribbons, *Phys. Rev. B* 86 (11) (2012) 115438–115441–8.
- [65] L. Jiao, L. Zhang, X. Wang, G. Diankov, H. Dai, Narrow graphene nanoribbons from carbon nanotubes, *Nature* 458 (7240) (2009) 877–880.